bioRxiv preprint doi: https://doi.org/10.1101/242693; this version posted January 4, 2018. The copyright holder for this preprint (which was not certified by peer review) is the author/funder. All rights reserved. No reuse allowed without permission.

A polymer probe-based system for high density, long-lasting electrophysiological recordings across distributed neuronal circuits

Jason E. Chung[1,2], Hannah R. Joo[1,2], Jiang Lan Fan[3], Daniel F. Liu[2,3], Alex H. Barnett[4], Supin Chen[5,6], Charlotte Geaghan-Breiner[2], Mattias P. Karlsson[7], Magnus Karlsson[7], Kye Y. Lee[5], Hexin Liang[2], Jeremy F. Magland[4], W. Hamish Mehaffey[2], Angela C. Tooker[5], Michael S. Brainard[2,8], Leslie F. Greengard[4,9], Vanessa M. Tolosa[5,6], Loren M. Frank[2,8]

Author Affiliations

[1] Medical Scientist Training Program and Neuroscience Graduate Program, University of California San Francisco, CA 94158, USA.

[2] Kavli Institute for Fundamental Neuroscience, Center for Integrative Neuroscience, and Department of Physiology, University of California San Francisco, CA 94158, USA.

[3] Bioengineering Graduate Program, University of California San Francisco, CA 94158, USA.

[4] Center for Computational Biology, Flatiron Institute, 162 Fifth Avenue, New York, NY 10010, USA.

[5] Center for Micro- and Nano-Technology, Lawrence Livermore National Laboratory, Livermore, CA 94550, USA.

[6] Current address: Neuralink Corp., San Francisco, CA 94107, USA.

[7] SpikeGadgets llc., San Francisco, CA 94158, USA.

[8] Howard Hughes Medical Institute

[9] Courant Institute, NYU, New York, NY 10012, USA.

Abstract

The brain is a massively interconnected neuronal network, organized into specialized circuits consisting of large ensembles of neurons distributed across anatomically connected regions. While circuit computations depend upon millisecond timescale interactions, the structure of the underlying networks are remodeled on timescales ranging from seconds to months. Current approaches lack the combination of resolution, spatial coverage, longevity, and stability to measure the detailed dynamics of these networks. Here we describe a large-scale, multisite recording platform that integrates polymer electrodes with a modular stacking headstage design supporting up to 1024 channels of recording in freely-behaving rats. We show that the

bioRxiv preprint doi: https://doi.org/10.1101/242693; this version posted January 4, 2018. The copyright holder for this preprint (which was not certified by peer review) is the author/funder. All rights reserved. No reuse allowed without permission.

integrated system can yield months-long recordings from hundreds of well-isolated units across multiple regions. Moreover, the recordings are stable enough to track a substantial fraction of single units for over a week. This platform enables large-scale electrophysiological interrogation of the function and evolution of distributed circuits throughout an animal's adult life.

Introduction

The ideal tool to observe brain dynamics would provide a minimally invasive, arbitrarily broad and high spatial and temporal resolution sampling of neural activity from awake, freely-behaving animals. In the spatial domain, such a tool would enable locally dense measurements of the activity of many neurons in each of a large number of connected brain regions located anywhere in the brain. This would make it possible examine the patterns of activity supporting both local and distributed neuronal computations. In the temporal domain, such a tool would enable precise and accurate measurements of neuronal activity 24 hours a day, seven days a week across a lifetime. This would make it possible to examine the continuous evolution of activity that occurs as the brain adapts to and learns from its experiences.

Currently available approaches compromise between strengths in the spatial and temporal domains. One and two photon imaging approaches can provide long-lasting, cell-type specific, and stable sampling of neuronal populations, but are limited in depth to at most a few millimeters below the cortical surface[1,2] or require the insertion of GRIN lenses that do substantial damage to more superficial regions in the target path(s)[3]. These approaches are also limited by the signal to noise and temporal resolution of the indicators[4], which currently make it difficult or impossible to infer the precise timing of single spikes in vivo. Further, as these approaches use high intensity light, it is not clear that they could support continuous 24/7 measurements without damage to the tissue.

Electrophysiological approaches provide excellent temporal resolution, but studies in awake, freely-behaving animals currently require a tradeoff among spatial coverage, spatial distribution, per-region unit yields, signal longevity, and signal stability. More traditional 3D silicon or micro wire arrays similarly allow for dense sampling of multiple regions simultaneously and for long periods of time, but are typically restricted to superficial regions, and the use of more than two large arrays is typically restricted to animals larger than rodents[5,6]. Furthermore, the use of a single channel per penetration makes isolation of single neurons more error-prone[7].

The recently developed silicon neuropixel probe[8] allows users to select 384 active recordings sites from 960 total sites, and has demonstrated the ability to sample multiple regions with the limitation that the targets be collinear. These probes have also demonstrated

bioRxiv preprint doi: https://doi.org/10.1101/242693; this version posted January 4, 2018. The copyright holder for this preprint (which was not certified by peer review) is the author/funder. All rights reserved. No reuse allowed without permission.

signal longevity of 8 weeks in rats, though documentation of the quantity of single-units, the stability of the probe, and the probe's ability to sample the same units over time are not available. It also remains unclear whether the acquisition hardware and cabling is compatible with continuous 24/7 recording across days. As such, that system may make it difficult to evaluate the quality of long-term tracking of individual neurons and thus may not support the study of long term changes in individual neurons' firing patterns. Finally, the design and fabrication of these complex integrated devices is very expensive, and it is unlikely that more than a few geometries will ever be available to the neuroscience community.

A complementary recent development provides a platform for continuous 24/7 recording from awake, freely-behaving animals, with the ability to track individual neurons over long periods of time[9]. However, the 64-channel, individually movable tetrode-based system lacks the ability to yield hundreds of well-isolated neurons, and it remains unclear whether the stability and cell tracking abilities will extend to larger and higher channel-count implants.

Flexible polymer devices have the potential to provide a platform that combines the density of contacts available in silicon devices with the modularity and longevity of microwire approaches. Polymer arrays provide a stable, long-lasting, and biocompatible neural interface[10-13], in part from counteracting micromotions of the array relative to the brain[14]. However, polymer arrays capable of resolving single neurons have largely existed at the single device and proof-of-concept stage[10,15-20]. Moreover, the insertion and implantation of flexible devices is markedly more complicated than that of their rigid counterparts, and are areas of active research with a diversity of approaches[21-27]. Consequently, the promise of these devices for high density, long lasting recordings has yet to be realized.

In this work, we introduce new, high density polymer probes integrated with a modular implantation platform and recording system. This system makes it possible to measure the activity of hundreds of single neurons across multiple, spatially distributed structures in freely-behaving animals. The system supports continuous 24/7 recording and yields high quality, large-scale single unit recordings for many months. Alongside the system, we adapt the MountainSort[28] spike sorting software to link clusters across time segments, and thereby demonstrate stable recordings from many individual neurons for over a week.

Results

Modular implantation platform

A fundamental aim of our implantation platform is that it can be used to collect data from different regions of a distributed neural circuit simultaneously, in an awake, freely-behaving

bioRxiv preprint doi: https://doi.org/10.1101/242693; this version posted January 4, 2018. The copyright holder for this preprint (which was not certified by peer review) is the author/funder. All rights reserved. No reuse allowed without permission.

animal, with minimal or no experiment-specific implantation components. This requires that recording electrodes be flexibly distributed across the brain, yet in high enough density within a region to yield many single units (putative single neurons). Currently, this requires a tradeoff between one or at most a few large, high-density arrays with rigid geometries, and many lower-density arrays (or single channels) able to be arbitrarily and precisely distributed across the brain. Our approach, outlined in Fig. 1A, reduces the need for this tradeoff, allowing for high-resolution sampling across multiple targeted regions.

Multishank polymer electrode arrays form the modular implantable unit. Each 32- or 64-ch polyimide array[29,30] consists of two or four shanks, with 16 channels per shank, each with electrically deposited PEDOT-PSS[31] (Fig. 1B). The 32 channel devices have an attached 32-channel omnetics connectors, two of which can be coupled to mating connectors attached to printed circuit board (PCB), which in turn is wire-bonded to a 64-channel amplifying, digitizing, and multiplexing chip (INTAN technologies). The 64-channel devices were directly wire-bonded to a similar PCB. The resulting 64-channel modules (Fig. 1C) can be stacked using mezzanine connectors and connected to a field programmable gate array (FPGA, SpikeGadgets LLC) which supports up to two stacks of eight modules, for a total of 1024-channels (Fig 1D). The FPGA synchronizes the modules, and converts the serial peripheral interface bus (SPI) signal from each module to high-definition multimedia interface (HDMI) format. The 1024 channel, 30 KHz / channel data is streamed via a micro-HDMI cable through a HDMI commutator to the data acquisition computer where it is visualized and saved (Fig. 1E). The ability to stream high speed data through a commutator is a key feature of our design that makes it possible to carry out long term recordings.

The flexibility of polyimide arrays, while providing benefits to biocompatibility[13], presents challenges to insertion. Additional structural support must be provided in order to successfully and accurately insert the probes, and in our application, this support must be compact enough for the dense packing of arrays (<1 mm between inserted probes). Here we take advantage of our previous development of a system including a detachable silicon stiffener. Arrays attached to stiffeners are inserted in series into brain tissue[21], and subsequently tethered to a custom 3d-printed base piece, which is contoured and anchored to the skull (Fig. S1; See Methods for detailed description of the implantation procedure). The rest of the implant is then assembled on the head, and includes layers of silicone gel and elastomer to protect the polymer arrays from damage and active electronic components from moisture, and custom 3d-printed casing and heatsinks for impact resistance and heat dissipation (Fig. S1).

bioRxiv preprint doi: https://doi.org/10.1101/242693; this version posted January 4, 2018. The copyright holder for this preprint (which was not certified by peer review) is the author/funder. All rights reserved. No reuse allowed without permission.

Recordings of hundreds of single units distributed across multiple regions.

Information processing in the brain is carried out by populations of many single neurons which span multiple regions. To demonstrate our platform's ability to resolve network events spanning many regions, we examined data from an animal implanted with the full 16 module system. Of these, 8 modules were used for single-unit recording (see methods for more details). Data were collected during a rest period in a familiar environment. Spike sorting using MountainSort[28] on data from these 512 channels 45 days after implantation produced 1533 clusters with a continuum of qualities. Three hundred seventy five of the 1533 clusters exceeded the conservative cluster quality metric thresholds (isolation > 0.96, noise overlap < 0.03) used previously[28], and are henceforth considered single units (Fig 2A). The modules used for single unit recording were distributed among medial prefrontal cortex (mPFC), orbitofrontal cortex (OFC), and ventral striatum (VS), and polymer probes designed for recording local field potentials (LFP) were targeted to the hippocampus (HPC) (Fig 2B).

The ability to examine ensembles of single units across multiple regions makes it possible to examine cross-area coordination. Here we focused on times when we detected hippocampal sharp wave-ripples (SWRs). The SWR[32] is an event of synchronous population activity known to influence activity across the majority of the brain[33]. Specifically, neurons across many cortical[34-38] and subcortical regions[39-41] show changes in firing rates around the time of SWRs.

Changes in activity across the population of 375 single units were evident during individual SWRs (Fig. 2C, D). Across all SWRs, these changes manifested as significant increases and decreases in firing of a subset of units in each region (Fig. 2E). Using a criterion of $p < 0.05$, we found that 19 of 61 mPFC (13 positively, 6 negatively) ($p<1.0e-4$ as compared to expected proportion, z-test for proportions), 27 of 118 NAc (24 positively, 3 negatively) ($p<1.0e-4$, z-test for proportions), and 28 of 196 OFC (18 positively, 10 negatively) ($p<1.0e-3$ z-test for proportions) units were significantly modulated at the time of SWRs (see Methods), Our results in mPFC and NAc are consistent with what has been seen previously in dual-site hippocampus and mPFC or NAc recordings during the resting state[40,42,43] where a majority of modulated units are excited during SWRs. Previous reports have not examined single unit-activity in OFC during SWRs, however, and here we report approximately twice as many modulated neurons as would be expected by chance, providing a further confirmation that SWRs events engage activity across many cortical regions.

Longevity of single-unit recording

bioRxiv preprint doi: https://doi.org/10.1101/242693; this version posted January 4, 2018. The copyright holder for this preprint (which was not certified by peer review) is the author/funder. All rights reserved. No reuse allowed without permission.

While polymer devices have shown promise in achieving a long-term biocompatible interface with neuronal tissue[10,15-20], their benefits have not yet been combined into configurations and systems capable of sampling many neurons simultaneously. To evaluate the long-term, high yield single-unit recording capabilities of polymer arrays we implanted three rats with polymer probes into mPFC or OFC for 160 days or more (one 72-ch implant, one 128-ch implant, and one 288-ch implant).

These implants yielded long lasting, high quality recordings (Fig. 3A), with some initial variability across a six-week timescale, consistent with the brain's recovery from an acute injury and the transition to a stable, chronic response (Supplementary Fig 2.). Subsequently, recording yield was stable until the end of recording (experiments terminated at 160 days to ensure the availability of histology), yielding up to 45 total units on an individual shank and ~1 single-unit per contact on average, with higher yields in mPFC as compared to OFC (Fig. 3A). Importantly, even after 160 days, our system continued to yield high amplitude, clearly distinguishable spikes, making it possible to maintain well isolated individual single units (Fig. 3B). In one case, we choose to leave one animal implanted for 253 days, at which time the experiment was terminated as the animal was reaching the end of expected lifespan. Here we found that high quality single unit recordings could be made across that entire span, albeit with a gradual decline in the number of well-isolated units (from 27 single-units at day 45 post-implant to 16 single-units at 253 days post-implant; Supplemental Fig 2C).

Stability of recording

The ability to track individual neurons across days depends upon stable recordings and a clustering strategy that can follow changes in waveform shape, which are thought to result largely from small movements of the electrodes relative to the tissue (termed "electrode drift"). We implanted six 32-channel probes, each with two 16-channel shanks (192 of 288 total implanted channels, see Methods) into each of three animals, and recorded continuously for 10 days, (animal A, day 53 to 63 post-implant, animal B, day 47 to 57 post-implant, animal C, day 42 to 52 post-implant). Here we illustrate tracking on one representative shank from one of these animals, although analyses of additional shanks are ongoing. In order to cluster the 1.6 TB of data per 16-ch shank, the data was divided into 10 segments of 24-hr length and clustered using MountainSort[28]. We developed a simple and conservative approach to identify clusters across segments based on a mutual nearest-neighbor rule (see methods). As expected[9], all putative neurons showed some degree of waveform variation across the 240 hours, even those that could be tracked across the entire time period (Fig. 4A-C). For this

bioRxiv preprint doi: https://doi.org/10.1101/242693; this version posted January 4, 2018. The copyright holder for this preprint (which was not certified by peer review) is the author/funder. All rights reserved. No reuse allowed without permission.

shank, 6 out of 17 clusters from the first 24-hour period could be tracked for over one week (Fig. 4D), and many units could be tracked across multiple days.

Polymer probe recording longevity and stability in the Songbird

Finally, we also demonstrated that our polymer devices and surgical implantation approach can be adapted for use in other species. We implanted a two-shank 32-channel polymer array into Zebra Finch Area X, a striatopallidal nucleus dedicated to song. When the bird sings song directed to females, individual neurons in this region discharge with high degrees of cross-trial reliability across song renditions (r values often > than 0.9) and these temporally precise patterns are not shared across units[44]. This precise song-locked neural activing during song allows us to compare both spike-waveforms, and song-related responses across days to asses recording stability.

We found that our arrays also performed very well in the songbird (Supplemental Fig. 3), with only minor adaptations in the implantation procedures. We obtained long lasting and high-quality single unit recordings for the length of the experiment (30 days; Fig. 5A). Further, units across days had similar waveforms and nearly identical firing patterns (Fig. 5B), strongly suggesting stable single unit recordings across multiple days; something that to our knowledge has not previously been achieved in this system.

Discussion

Electrophysiological recordings provide high temporal resolution information about the activity of neurons, and our system makes it possible to acquire this high temporal resolution information simultaneously across many neurons within a region and across many regions, and to do so across long periods. We demonstrated large scale recordings from neurons in three widely separated brain regions, the OFC, the mPFC and the NAc, yielding a conservative total of 375 well isolated neurons recorded simultaneously. Moreover, we found that high quality recordings could be obtained across many months. In addition, our system makes it possible to do continuous, 24 hours per day, 7 days a week recording, and with a simple and conservative linking algorithm we could track many single units across more than a week. We also demonstrated long lasting recordings in the songbird. Our approach is highly complementary to that of the recently reported neuropixels probe, and the combination of features of our system, density, modularity, longevity and stability, will enable experimenters to ask and answer new questions about how the brain works.

bioRxiv preprint doi: https://doi.org/10.1101/242693; this version posted January 4, 2018. The copyright holder for this preprint (which was not certified by peer review) is the author/funder. All rights reserved. No reuse allowed without permission.

Density and Modularity. Neural computations depend on local circuits, distributed circuits within a brain region, and widely distributed circuits located across regions. Measuring the activity patterns underlying those computations requires sampling many neurons across all three scales. The individual polymer arrays consist of multiple single shanks, each with 16 closely spaced electrode contacts. This geometry allows us to take advantage of the higher quality single unit isolation available when multiple electrodes detect signals from the same neurons[45] while still sampling from a relatively large local region of the brain. Further, our current devices have two or four shanks, making it possible to record across multiple closely spaced sites in the same brain region. These densities resulted in recordings of up to 45 well isolated single units on a single shank and on average one unit per recording electrode when devices were placed in neocortex. As a result, our arrays permit study of local circuit dynamics in the neighborhood of a shank and, simultaneously, across shanks in the same brain region.

Here we note that while it is tempting to compare recording yields across devices, these comparisons can only be done fairly if the same spike sorting approach was applied in both cases. We used our recently developed fully automatic spike sorting package MountainSort[28] and applied conservative cluster quality metrics to ensure that we were only including very well isolated units. Nonetheless, these per-channel yields are similar to those reported recently for an acute implantation of two Neuropixels probes, where ~370 units per probe were recorded from the 384 active sites. A direct comparison of the yields of chronically implanted Neuropixel probes is not possible because those values were not reported.

Our approach was also designed to be modular so that an experimenter could flexibly target a large number of high density recording devices to multiple regions located anywhere in the brain. As a result, multiple probes can be implanted in a single region, enabling higher densities within region, and sets of probes can be implanted across regions, enabling high density recordings across distributed circuits. We illustrated these capabilities with recordings from 375 units distributed across mPFC, OFC and NAc, selected from 1533 identified clusters. These recordings allowed us to identify a subset of SWR-modulated OFC neurons and simultaneous modulations of brain activity during hippocampal SWRs across regions. Recordings from populations of this size make it possible to carry out a number of analyses that are either not possible or very difficult with lower unit counts, including simultaneous comparisons of activity patterns across regions. In this respect only the Neuropixels probe offers similar recording densities, and there the linear arrangement of sites may limit the density of recordings within a single region.

bioRxiv preprint doi: https://doi.org/10.1101/242693; this version posted January 4, 2018. The copyright holder for this preprint (which was not certified by peer review) is the author/funder. All rights reserved. No reuse allowed without permission.

Other available technologies can yield high unit counts in specialized circumstances, as where implants of 40 individually moveable tetrodes yielded high unit counts (~250) in the hippocampus[46]. We note, however, that those high yields are only possible in regions with high-density cell body layers. Further, targeting many regions with tetrodes requires custom built microdrive arrays, and size, weight and connector considerations limit the total number of tetrodes that could be used in one animal, and likely influence the overall stability of the implanted arrays. Finally, our polymer probes require no manual adjustment but can still produce very long-lasting recordings, saving substantial experimenter time and effort.

Longevity and Stability. Experiences drive plasticity in neural circuits which changes the way they process information. These changes manifest on many timescales, from seconds to months, and our system provides the capacity to measure those changes in neural populations in both local and more distributed circuits. We were able to maintain high quality recordings for 160 days across multiple animals and multiple implanted devices, and extended one set of recordings out to 283 days with only a very gradual decline in recording quality.

This longevity far exceeds that of previous generations of chronically implanted silicon devices, where recording quality generally declines quickly after implantation, requiring the use of microdrives so that the devices could be periodically advanced into fresh tissue[47]. As a result, previous use of very high-density silicon devices was either limited to acute recordings in mice[48], or at lower densities with microdrives in chronic applications. The relatively rare instances of implantation of immobile silicon devices for chronic application have shown mixed results[49-51]. The consistent high-quality recordings for 160 days also exceed those reported for the immobile, chronically-implanted neuropixels device, where stable total firing rates and un-curated cluster numbers were reported for recordings spanning 56 days[8], although those devices may yield much longer recordings than reported. We note, however, that once again a direct comparison would require the same spike sorting approach, and as the methods used for the neuropixel probe include setting a detection threshold and an initial number of clusters based on recording session-specific measurements[52], direct comparisons are difficult.

Finally, we were also able to demonstrate a level of stability of recordings that makes it possible to study the same units, 24 hours a day across at least a week. Using a simple and fully automatic algorithm for matching clustered units across days, we found that we could track ~20% of units for seven or more days. Importantly, we note here that our quantification and electrode-drift tracking method provides a conservative estimate of trackable units, and that given the simplicity of our algorithm, it is likely that a more sophisticated approach would allow

bioRxiv preprint doi: https://doi.org/10.1101/242693; this version posted January 4, 2018. The copyright holder for this preprint (which was not certified by peer review) is the author/funder. All rights reserved. No reuse allowed without permission.

for even better results. We were also able to identify units with very similar waveforms and coding properties across days in the songbird, suggesting that we were recording from the same units across days there as well.

The proportion of units we could track across more than a week is similar to that recently reported for a semi-automatic method applied to data from 64 channel, 16-tetrode based system[9]. That system yielded an average total of 19 units per day, however, and the more than an order of magnitude increase in the number of units we can measure on a given day yields a concomitant increase in the number of units that can be tracked over long time periods. That will make it possible to monitor experience- or time-driven changes across larger populations and across multiple regions simultaneously.

In summary, our system enables the use of large scale polymer recording arrays in other small animals, and brings with it higher channel counts, cell yields, and longevities for chronically-implanted animals. In larger animals, where larger impact forces and brain pulsations are present, flexible polymer will likely match or exceed performance of existing technologies. Utilization of the full 22 mm x 22 mm x 25 mm 1024-ch system should be relatively straightforward, capable of fitting into existing primate chambers. More so, multiple 1024-ch systems could be used given appropriate animal size and housing.

The implantation platform will benefit from upcoming silicon and polymer process advances, driving higher channel counts, lower power consumption, and smaller implant sizes. Beyond pure recording applications, the modular design lends itself to integration with new elements that expand the functionality, such as other recording capabilities[53], circuit manipulations[54,55], and computational power for closed-loop applications. Further, because our approach separates the recording device from the silicon chip that amplifies and digitizes the signals, it provides a cost-effective platform for developing different array designs for different brain regions or species.

Figure Legends

Figure 1. Modular 1024-channel implantation platform overview. (A) Data path from electrode to computer, with box color corresponding to related components in following subfigures. (B) Polymer electrode array. Left, schematic of 16-channel shank of polymer array designed for single-unit recording. Shank is 14 µm thick. Middle-left, image of 16-ch shank. Middle-right, 4-shank (250 µm edge-to-edge spacing), 64-channel array. Right, full polymer

bioRxiv preprint doi: https://doi.org/10.1101/242693; this version posted January 4, 2018. The copyright holder for this preprint (which was not certified by peer review) is the author/funder. All rights reserved. No reuse allowed without permission.

array, bond pads at top of array. (C) Left, view of individual 64-channel module with amplifying, digitizing, and multiplexing chip (Intan Technologies) wire-bonded onto board, and mezzanine-style connector attached at top of board. Right, two modules stacked together. (D) Full 1024-channel, 16-module, recording system stacked into FPGA headstage (SpikeGadgets llc) during implantation. (E) Raw 100 ms traces from one 16-ch shank. Scalebar corresponds to 1 mv.

Figure 2. Large-scale, distributed recording. (A) Number of putative single-unit clusters from 512 channels (of the 1024-channel implant), stratified by quality metric thresholds. Automated curation using MountainSort (noise overlap 0.03, isolation 0.96, dotted lines) resulted in the identification of 375 single units from the 512 channels. (B) Schematic of the rat brain with targeted regions highlighted. (C) Top, 5 second raw LFP trace from one of 128 channels implanted into Hippocampus, centered on a SWR. Middle, 150 – 250 Hz filtered trace. Bottom, spike rasters from 375 simultaneously recorded neurons from the same time period, with colors corresponding to the highlighted region. Horizontal axis in ms. (D) As in (C), but for 1 second centered around the same event. (E) Averaged traces for average LFP (top), power (middle, 150 – 250 Hz). Bottom, normalized firing rate, peri-SWR histograms for the same 375 simultaneously recorded single neurons as in (C, D), separated by recording location, and ordered by time of trough or time of peak (calculated from 660 SWRs).

Figure 3. Single-unit recording yield of polymer probes over time. (A) Single-unit yields for polymer probes per channel (left y-axis) or per 16-ch shank (right y-axis) over 160 days post-implantation (x-axis) in rats. Solid line is the mean cell yield across 8 shanks, dotted lines ± 1 SE. Individual time points per shank are shown as color-coded dots by region. (B) Waveforms for units clustered for data point with green arrowhead. Scale bar corresponds to 200 µv and 2 ms.

Figure 4. Tracking individual single-units over time. (A-C) Example neuron tracked for 10 days of continuous recording. (A) Geometric layout of recording channels, with 3 boxed channels on which the unit was clustered. (B) Average waveforms on subset of channels in indicated 10-hour time bin. Scale bar corresponds to 400 µv and 1 ms. (C) Spike amplitude over time, for all ~600,000 events in the time period. (D) Period over which each cluster could be tracked (same shank as in (A-C)).

bioRxiv preprint doi: https://doi.org/10.1101/242693; this version posted January 4, 2018. The copyright holder for this preprint (which was not certified by peer review) is the author/funder. All rights reserved. No reuse allowed without permission.

Figure 5. Single-unit recording in the zebra finch. (A) Single-unit yields for polymer probes per channel (left y-axis) or per 16-ch shank (right y-axis) over 30 days post-implantation (x-axis) in area X of a zebra finch. Gaps represent days where data were not collected. (B) Top, spectrogram of song. Below, rasters for one putative single-unit found across 3 days. (C) Waveforms for the same example unit shown in (B), corresponding to the 3 highlighted channels. Scalebar corresponds to to 250 μv and 1 ms.

Supplemental Figure 1. Surgical approach and implant construction. (A, B) Top-down views of a rat skull with 3-D printed implant base attached (A) before polymer array insertion, and (B) after insertion of 7 polymer probes. (C) Magnified view of polymer probes entering into brain. (D) Cross-sectional schematic of implant after arrays have been inserted and silicone gel has been added to the 3-D printed base, and (E) of the assembled implant, with silicone elastomer fill to protect soft passive electrical components and moisture-sensitive active electrical components, and to provide strain relief for their soft-hard interface. (F) 3-D model of active electronics (red) and casing (grey), which provide structural support and protection for the passive electrical connection from the implanted contacts to the active electronic components. (G) 3-D model of full implant with polymer probe (cyan), single 64-ch board module (green), active electronics and micro-HDMI cable (red). (H) Rat implanted with full system, including heat sinks (black) and silicone grommets for impact resistance (cyan).

Supplemental Figure 2 (corresponding to Fig. 3). Histology 160 days after implantation. Histology shown corresponds to shank with green arrowhead in Fig 3A. (A) Merged image with glial fibrillary acidic protein (GFAP) stain in green, and NeuroTrace (ThermoFisher Scientific) in blue (B) As in (A), but for highlighted region. Left, merge, middle, GFAP, right, NeuroTrace. (C) Cell yields per channel (left y-axis) or per 18-ch shank (right y-axis) for a probe implanted for 283 days. Experiment was terminated due to animal approaching end of expected lifespan.

Supplemental Figure 3 (corresponding to Fig. 5). Raw data from a zebra finch on day 30 post-implantation. (A) Top, Spectrogram of song. Below, raw traces for the two channels marked to the right.

bioRxiv preprint doi: https://doi.org/10.1101/242693; this version posted January 4, 2018. The copyright holder for this preprint (which was not certified by peer review) is the author/funder. All rights reserved. No reuse allowed without permission.

Methods

Rat

All experiments were conducted in accordance with University of California San Francisco Institutional Animal Care and Use Committee and US National Institutes of Health guidelines. Rat datasets were collected from male long-evans rats (RRID: RGD_2308852), 6-23 months of age, with weights ranging from 500-600 g. All rats were fed standard rat chow (LabDiet 5001) in addition to sweetened evaporated milk for reward during behavioral performance. Rats were ordered from Charles River Laboratories at weights of 300-400 g and 3-4 months of age.

Surgical implantation

Male long-evans rats (RRID: RGD_2308852), were implanted with polymer probe(s) at 6-12 months of age. Polymer arrays were targeted to a variety of targets (all coordinates given in millimeters relative to bregma: medial prefrontal cortex (mPFC, including prelimbic and anterior cingulate cortices; ±1.2 ML, +1.5 to +4.5 AP, -2.0 to -4.0 DV, 6-8° from saggital), ventral striatum (VS, primarily nucleus accumbens shell; ±0.7 to +1.9 ML, +0.8 to +1.9 AP, -7.2 DV), orbitofrontal cortex (OFC, primarily lateral orbitofrontal cortex; ±3.5 to 3.7 ML, +2.6 to +3.4 AP), dorsal hippocampus (dHPC, ±2.3 to 2.8 ML, -3.5 to -4.0 AP, -4.0 to -6.0 DV). For some subjects, stimulating electrodes and tetrode microdrives were also implanted at the same time, targeted to the ventral hippocampal commissure (vHC, ±1.0 ML, -1.2 or -2.0 AP) and dHPC.

Anesthesia was induced using ketamine, xylazine, atropine, and isoflurane. Every 4 hours, the animal received additional Ketamine, xylazine, and atropine.

The skull was cleaned, targets were marked, and all drilling was completed. Commercially-pure titanium (CpTi) 0-80 set screws (United Titanium, OH) were then placed around the perimeter of the implant due to its well-known ability to osseo-integrate[56]. Bone dust was then cleared from the skull, and craniectomies and durectomies were completed. The skull was then briefly allowed to dry and a custom 3d-printed base piece (See key resources table for files, RGD837 Stratasys, MN) was then fixed to the skull using 4-META/MMA-TBB[57] (C&B Metabond). This base piece serves a multitude of functions including a reservoir for saline or silicone gel, an anchoring point for the polymer arrays, and a standardized interface from which the rest of the implant can be affixed and constructed during the implantation.

Polymer probes attached to silicon stiffeners using polyethylene glycol (PEG) were then inserted to the brain[21] using custom 3d-printed pieces (see key resources), avoiding surface vasculature. Polymer probes were then affixed via a piece of polyimide to the 3d-printed base

bioRxiv preprint doi: https://doi.org/10.1101/242693; this version posted January 4, 2018. The copyright holder for this preprint (which was not certified by peer review) is the author/funder. All rights reserved. No reuse allowed without permission.

piece before PEG was dissolved using saline, and silicon stiffeners were retracted. Gentle bends were allowed to form below the anchoring points on the polymer arrays, acting as strain relief. Insertion was repeated for all targeted locations.

After all polymer probes were affixed, the saline filling the 3d-printed base piece was then removed and silicone gel (Dow-Corning 3-4680) was used to fill the 3d-printed base piece, providing a means to seal the durectomies and craniectomies, and also provide added support for the polymer arrays. Additional custom 3d-printed pieces were used to construct a protective case around the polymer devices and active electronic components of the implant. Silicone elastomer (Quik-sil, WPI) was then added to the remainder of the exposed polymer, with special attention to the soft polymer – rigid printed circuit board interface, and 3d-printed casing was affixed to the skull using dental acrylic.

Polymer arrays

The polymer arrays were fabricated at the Lawrence Livermore National Laboratory nanofabrication facility as described previously[29,30]. Briefly, devices have three trace metal layers and four polyimide layers with a total device thickness of 14 µm.

Devices with an LFP configuration had 20 µm contacts in a single-line with a center-to-center distance of 100 µm, tapered shank width of 61 µm to 80 µm, 21 or 22 contacts per shank, and an edge-of-shank to edge-of-shank distance of 420 µm.

Devices with a 4-shank, 64-channel single-unit configuration are diagrammed in Fig. 1, and had an edge-of-shank to edge-of-shank distance of 250 µm. Devices with a 2-shank, 32-channel single unit configuration had an identical shank layout to the 4-shank configuration with the notable reduction in edge-of-contact to edge-of-shank distance from 12 µm (4-shank design) to 6 µm (2-shank design).

The device with a 2-shank, 36-channel single-unit configuration (featured in Supplemental Fig. 2) had a similar dual-line, staggered design to the other single-unit configurations with a few notable exceptions. The shank width was 100 µm, edge-of-contact to edge-of-shank distance was 12 µm, and 3 of the 18 contacts were placed closer to the tip of the shank.

16-module, 1024-channel implant

The 16-modules were distributed equally across both hemispheres. Of the 16 modules implanted, 2 were targeted to dHPC and of an LFP configuration. Of the remaining 14 modules,

bioRxiv preprint doi: https://doi.org/10.1101/242693; this version posted January 4, 2018. The copyright holder for this preprint (which was not certified by peer review) is the author/funder. All rights reserved. No reuse allowed without permission.

4 were targeted to OFC, 4 were targeted to VS, and 6 were targeted to mPFC. There were device failures on 4/6 targeted to mPFC, and 2/4 targeted to VS.

160 day periodic recordings

Polymer probes were targeted to mPFC or OFC. In one implant, two two-shank 36-channel arrays were implanted into mPFC and recorded from for 263 days, the termination of the experiment due to animal approaching end of life expectancy. This animal was recorded from using the NSpike data acquisition system (L.M.F. and J. MacArthur, Harvard Instrumentation Design Laboratory) in a 13'' x 13'' rest box, and was returned to its home cage. The second implant consisted of four two-shank 32-channel arrays, all targeted to OFC. The third animal was implanted with six, two-shank, 32-channel polymer arrays targeted to mPFC, alongside two stimulating electrodes targeted to vHC, and 24 tetrodes targeted to dHPC bilaterally, for a total of 288-channels of recording. For the longevity analyses, the second and third animals were also recorded from in a 13'' x 13'' rest box, but on some unanalyzed days, recordings were also carried out while the animal ran in a spatial environment.

10-day continuous recording in mPFC

Three animals were implanted with six, two-shank, 32-channel polymer arrays targeted to mPFC, alongside two stimulating electrodes targeted to vHC, and 24 tetrodes targeted to dHPC bilaterally. One of the three animals also had one four-shank, 64-channel polymer array targeted to right OFC. This same animal had a device failure resulting in two functional 32-channel polymer arrays in mPFC and one 64-channel polymer array in OFC. Recordings were carried out while animals were housed in their home cages and in alternating epochs of exposure to a familiar rest box and one of two spatial environments. Animals ran 600 – 1000 meters per day in these spatial environments. This provided a challenging experimental setting in which to assess recording stability.

Spike sorting

Clustering was done using MountainSort, using settings and thresholds as reported previously[28]. Adjacency radius was set to 100 µm when sorting the 20 µm contact, 20 µm edge-to-edge dual-line designs, resulting in clustering neighborhoods of 5 to 9 electrodes. The event detection threshold was set to 3 SD. Putative single-units were identified using previously set thresholds (isolation > 0.96, noise overlap < 0.03) and an automatic merging procedure, reported previously[28], was used to identify pairs of clusters that corresponded to the higher and

bioRxiv preprint doi: https://doi.org/10.1101/242693; this version posted January 4, 2018. The copyright holder for this preprint (which was not certified by peer review) is the author/funder. All rights reserved. No reuse allowed without permission.

lower amplitude components of single units that fired in bursts with decrementing spike amplitudes.

For the 240-hr continuous recording datasets, filtering and spatial whitening was applied to the entire 240-hr recording, and then data was clustered in 24-hour segments. Automated curation and bursting-related merging was first completed independently for each segment. As a result, all clusters in all segments satisfied our criteria for well isolated units. Linking clusters between segments was done using a mutual nearest neighbor rule. For every cluster in the first segment, a 1.66 ms spatially-whitened waveform template was calculated from the last 1000 events, using every channel on the shank. Similarly, for every cluster in the second segment, a waveform template was calculated from the first 1000 events. Next, the L^2 distance was calculated between every segment 1 and segment 2 pair of templates. If cluster A from segment 1 and cluster A' from segment 2 were mutual nearest neighbors, then the segments were linked.

This approach was successful for three reasons. First, it used only well isolated clusters from each segment, and only matched these well isolated clusters. Second, because the 24-hour segments were not aligned to specific events in the animals' lives, and thus partitioned the spiking activity at points where large, sudden changes in spike amplitudes were very unlikely. Third, the distance calculation was based on whitened spike waveforms from the entire 16 electrode array, yielding unique templates for each unit. The mutual nearest neighbor calculation ensured that these templates matched across the segment boundaries, and in practice we found that this linking algorithm yielded plots of spike amplitude over time that were continuous across the period where the unit could be tracked.

SWR detection and modulation

SWRs were detected as previously described[58]. Briefly, LFPs from a contact near CA1 was filtered into the ripple band (150 – 250 Hz) and the envelope of band-passed LFPs was determined by Hilbert transform. SWR were initially detected when the envelope exceeded a threshold (mean + 3 SD) on the contact. SWR events were defined as times around the initially detected events during which the envelope exceeded the mean. For SWR-trigged firing rates, only SWRs separated by at least 500 ms were included.

SWR modulation analysis was carried out as described previously[36]. Briefly, spikes were aligned to SWR onset resulting in SWR-aligned rasters. Cells with less than 50 spikes in the SWR-aligned rasters were excluded from these analyses. To determine the significance of SWR modulation, we created 1,000 shuffled rasters by circularly shifting spikes with a random jitter around each SWR, and defined a baseline response as the mean of all shuffled responses. We

bioRxiv preprint doi: https://doi.org/10.1101/242693; this version posted January 4, 2018. The copyright holder for this preprint (which was not certified by peer review) is the author/funder. All rights reserved. No reuse allowed without permission.

then compared the response in a 0-200 ms window after SWR onset (SWR response) to the baseline. We considered a cell as SWR-modulated when the mean squared difference of its shuffled response from the baseline (i.e., $p < 0.05$). SWR-modulated neurons were further categorized as SWR-excited or SWR-inhibited by comparing the rate in a 0-200 ms window after SWR onset, with the rate of the mean shuffled response in the same 0-200 ms window.

Zebra finch

Adult (> 190 posthatch days) male zebra finches (Taeniopygia guttata) raised in our colony were used for electrophysiology in this study. All procedures were performed in accordance with protocols approved by the University of California, San Francisco (UCSF) Institutional Animal Care and Use Committee.

Surgical procedure (Zebra finch)

Birds were deprived of food and water for 1 h and then anesthetized with an intramuscular injection of 30–40 µl of equithesin (0.85 g of chloral hydrate, 0.21 g of pentobarbital, 0.42 g of MgSO4, 2.2 ml of 100% ethanol, and 8.6 ml of propylene glycol to a total volume of 20 ml with water). Probes were implanted using the same custom printed pieces and procedures used in rodent (see key resources) however rather than the custom printed base piece, a small reservoir for saline was fashioned out of dental acrylic around the implanted probe to enhance separation from the stiffener. Probes were targeted stereotaxically to Area X, (5.2mm anterior, 1.7mm lateral to the posterior border of the divergence of the central sinus, 3.2mm deep). A ground electrode was implanted in the contralateral hemisphere, or cerebellum. Polymer probes were coated with silicone elastomer (Quik-sil. WPI), and the Omnetics connector was secured to the skull with dental cement.

Electrophysiology and data collection (Zebra finch)

For recording, a custom low-profile multiplexing headstage using an INTAN 2132 chip (Intan Technologies, Los Angeles, CA), was connected through a low-torque commutator (Dragonfly, Ridgeley WV). The acoustic signal was recorded by a small microphone located above the birdcage and amplified and bandpass filtered between 150 Hz and 15 kHz (Digikey, MN), and fed into an INTAN acquisition board. Electrophysiological and acoustic signals were digitized at 20-30kH, and recorded using the INTAN recording software. Songs were elicited by presentation of a female (e.g. ‘Directed’ song). Spikes were detected and sorted using

bioRxiv preprint doi: https://doi.org/10.1101/242693; this version posted January 4, 2018. The copyright holder for this preprint (which was not certified by peer review) is the author/funder. All rights reserved. No reuse allowed without permission.

MountainSort[28], with the same parameters used in rodent (100um adjacency radius, isolation > 0.96).

References

1 Helmchen, F., Denk, W. & Kerr, J. N. Miniaturization of two-photon microscopy for imaging in freely moving animals. *Cold Spring Harbor protocols* **2013**, 904-913, doi:10.1101/pdb.top078147 (2013).

2 Helmchen, F., Fee, M. S., Tank, D. W. & Denk, W. A miniature head-mounted two-photon microscope. high-resolution brain imaging in freely moving animals. *Neuron* **31**, 903--912 (2001).

3 Ghosh, K. K. *et al.* Miniaturized integration of a fluorescence microscope. *Nat Methods* **8**, 871-878, doi:10.1038/nmeth.1694 (2011).

4 Chen, T. W. *et al.* Ultrasensitive fluorescent proteins for imaging neuronal activity. *Nature* **499**, 295-300, doi:10.1038/nature12354 (2013).

5 Schwarz, D. A. *et al.* Chronic, wireless recordings of large-scale brain activity in freely moving rhesus monkeys. *Nat Methods* **11**, 670-676, doi:10.1038/nmeth.2936 (2014).

6 Mitz, A. R. *et al.* High channel count single-unit recordings from nonhuman primate frontal cortex. *J Neurosci Methods* **289**, 39-47, doi:10.1016/j.jneumeth.2017.07.001 (2017).

7 Wood, F., Black, M. J., Vargas-Irwin, C., Fellows, M. & Donoghue, J. P. On the variability of manual spike sorting. *IEEE Trans Biomed Eng* **51**, 912-918, doi:10.1109/TBME.2004.826677 (2004).

8 Jun, J. J. *et al.* Fully integrated silicon probes for high-density recording of neural activity. *Nature* **551**, 232-236, doi:10.1038/nature24636 (2017).

9 Dhawale, A. K. *et al.* Automated long-term recording and analysis of neural activity in behaving animals. *eLife* **6**, doi:10.7554/eLife.27702 (2017).

10 Luan, L. *et al.* Ultraflexible nanoelectronic probes form reliable, glial scar-free neural integration. *Sci Adv* **3**, e1601966, doi:10.1126/sciadv.1601966 (2017).

11 Jeong, J. W. *et al.* Soft materials in neuroengineering for hard problems in neuroscience. *Neuron* **86**, 175-186, doi:10.1016/j.neuron.2014.12.035 (2015).

12 Kim, T. I. *et al.* Injectable, cellular-scale optoelectronics with applications for wireless optogenetics. *Science* **340**, 211-216, doi:10.1126/science.1232437 (2013).

13 Lee, H. C. *et al.* Histological evaluation of flexible neural implants; flexibility limit for reducing the tissue response? *J Neural Eng* **14**, 036026, doi:10.1088/1741-2552/aa68f0 (2017).

14 Gilletti, A. & Muthuswamy, J. Brain micromotion around implants in the rodent somatosensory cortex. *J Neural Eng* **3**, 189-195, doi:10.1088/1741-2560/3/3/001 (2006).

15 Xie, C., Liu, J., Dai, X., Zhou, W. & Lieber, C. M. Three-dimensional macroporous nanoelectronic networks as minimally invasive brain probes. *Nature Materials* **14**, 1286-1292, doi:doi:10.1038/nmat4427 (2015).

bioRxiv preprint doi: https://doi.org/10.1101/242693; this version posted January 4, 2018. The copyright holder for this preprint (which was not certified by peer review) is the author/funder. All rights reserved. No reuse allowed without permission.

16 Kuo, J. T. *et al.* Novel flexible Parylene neural probe with 3D sheath structure for enhancing tissue integration. *Lab Chip* **13**, 554-561, doi:10.1039/c2lc40935f (2013).

17 Rodger, D. C. *et al.* Flexible parylene-based multielectrode array technology for high-density neural stimulation and recording. *Sensor Actuat B-Chem* **132**, 449-460, doi:10.1016/j.snb.2007.10.069 (2008).

18 Seo, D. *et al.* Wireless Recording in the Peripheral Nervous System with Ultrasonic Neural Dust. *Neuron* **91**, 529-539, doi:10.1016/j.neuron.2016.06.034 (2016).

19 Seo, D., Carmena, J. M., Rabaey, J. M., Maharbiz, M. M. & Alon, E. Model validation of untethered, ultrasonic neural dust motes for cortical recording. *J Neurosci Methods* **244**, 114-122, doi:10.1016/j.jneumeth.2014.07.025 (2015).

20 Tooker, A. *et al.* Towards a large-scale recording system: demonstration of polymer-based penetrating array for chronic neural recording. *Conf Proc IEEE Eng Med Biol Soc* **2014**, 6830-6833, doi:10.1109/EMBC.2014.6945197 (2014).

21 Felix, S. H. *et al.* Insertion of flexible neural probes using rigid stiffeners attached with biodissolvable adhesive. *Journal of visualized experiments : JoVE*, e50609, doi:10.3791/50609 (2013).

22 Zhou, T. *et al.* Syringe-injectable mesh electronics integrate seamlessly with minimal chronic immune response in the brain. *Proc Natl Acad Sci U S A* **114**, 5894-5899, doi:10.1073/pnas.1705509114 (2017).

23 Fu, T. M. *et al.* Stable long-term chronic brain mapping at the single-neuron level. *Nature Methods* **13**, 875-+, doi:10.1038/nmeth.3969 (2016).

24 Khilwani, R. *et al.* Ultra-miniature ultra-compliant neural probes with dissolvable delivery needles: design, fabrication and characterization. *Biomed Microdevices* **18**, 97, doi:10.1007/s10544-016-0125-4 (2016).

25 Wu, F. *et al.* Silk-Backed Structural Optimization of High-Density Flexible Intracortical Neural Probes. *J Microelectromech S* **24**, 62-69, doi:10.1109/Jmems.2014.2375326 (2015).

26 Jorfi, M., Skousen, J. L., Weder, C. & Capadona, J. R. Progress towards biocompatible intracortical microelectrodes for neural interfacing applications. *Journal of Neural Engineering* **12**, doi:Artn 011001
10.1088/1741-2560/12/1/011001 (2015).

27 Ware, T., Simon, D., Rennaker, R. L. & Voit, W. Smart Polymers for Neural Interfaces. *Polym Rev* **53**, 108-129, doi:10.1080/15583724.2012.751924 (2013).

28 Chung, J. E. *et al.* A Fully Automated Approach to Spike Sorting. *Neuron* **95**, 1381-1394 e1386, doi:10.1016/j.neuron.2017.08.030 (2017).

29 Tooker, A. *et al.* Polymer neural interface with dual-sided electrodes for neural stimulation and recording. *Conf Proc IEEE Eng Med Biol Soc* **2012**, 5999-6002, doi:10.1109/EMBC.2012.6347361 (2012).

30 Tooker, A. *et al.* Optimization of multi-layer metal neural probe design. *Conf Proc IEEE Eng Med Biol Soc* **2012**, 5995-5998, doi:10.1109/EMBC.2012.6347360 (2012).

31 Ludwig, K. A., Uram, J. D., Yang, J., Martin, D. C. & Kipke, D. R. Chronic neural recordings using silicon microelectrode arrays electrochemically deposited with a poly(3,4-ethylenedioxythiophene) (PEDOT) film. *J Neural Eng* **3**, 59-70, doi:S1741-2560(06)12912-2 [pii]

bioRxiv preprint doi: https://doi.org/10.1101/242693; this version posted January 4, 2018. The copyright holder for this preprint (which was not certified by peer review) is the author/funder. All rights reserved. No reuse allowed without permission.

10.1088/1741-2560/3/1/007 (2006).

32 Buzsaki, G. Hippocampal sharp wave-ripple: A cognitive biomarker for episodic memory and planning. *Hippocampus* **25**, 1073-1188 (2015).

33 Logothetis, N. K. *et al.* Hippocampal-cortical interaction during periods of subcortical silence. *Nature* **491**, 547-553, doi:10.1038/nature11618 (2012).

34 Chrobak, J. J. & Buzsaki, G. High-frequency oscillations in the output networks of the hippocampal-entorhinal axis of the freely behaving rat. *J Neurosci* **16**, 3056-3066 (1996).

35 Isomura, Y. *et al.* Integration and segregation of activity in entorhinal-hippocampal subregions by neocortical slow oscillations. *Neuron* **52**, 871-882 (2006).

36 Jadhav, S. P., Rothschild, G., Roumis, D. K. & Frank, L. M. Coordinated Excitation and Inhibition of Prefrontal Ensembles during Awake Hippocampal Sharp-Wave Ripple Events. *Neuron* **90**, 113-127, doi:10.1016/j.neuron.2016.02.010 (2016).

37 Ji, D. & Wilson, M. A. Coordinated memory replay in the visual cortex and hippocampus during sleep. *Nat Neurosci* **10**, 100-107 (2007).

38 Sirota, A., Csicsvari, J., Buhl, D. & Buzsaki, G. Communication between neocortex and hippocampus during sleep in rodents. *Proc Natl Acad Sci USA* **100**, 2065--2069 (2003).

39 Dragoi, G., Carpi, D., Recce, M., Csicsvari, J. & Buzsaki, G. Interactions between hippocampus and medial septum during sharp waves and theta oscillation in the behaving rat. *J Neurosci* **19**, 6191--6199 (1999).

40 Lansink, C. S., Goltstein, P. M., Lankelma, J. V., McNaughton, B. L. & Pennartz, C. M. Hippocampus leads ventral striatum in replay of place-reward information. *PLoS Biol* **7**, e1000173, doi:10.1371/journal.pbio.1000173 (2009).

41 Pennartz, C. M. *et al.* The ventral striatum in off-line processing: ensemble reactivation during sleep and modulation by hippocampal ripples. *J Neurosci* **24**, 6446--6456 (2004).

42 Wierzynski, C. M., Lubenov, E. V., Gu, M. & Siapas, A. G. State-dependent spike-timing relationships between hippocampal and prefrontal circuits during sleep. *Neuron* **61**, 587-596 (2009).

43 Tang, W., Shin, J. D., Frank, L. M. & Jadhav, S. P. Hippocampal-Prefrontal Reactivation during Learning Is Stronger in Awake Compared with Sleep States. *J Neurosci* **37**, 11789-11805, doi:10.1523/JNEUROSCI.2291-17.2017 (2017).

44 Woolley, S. C., Rajan, R., Joshua, M. & Doupe, A. J. Emergence of context-dependent variability across a basal ganglia network. *Neuron* **82**, 208-223, doi:10.1016/j.neuron.2014.01.039 (2014).

45 Gray, C. M., Maldonado, P. E., Wilson, M. & McNaughton, B. Tetrodes markedly improve the reliability and yield of multiple single- unit isolation from multi-unit recordings in cat striate cortex. *J Neurosci Methods* **63**, 43-54 (1995).

46 Pfeiffer, B. E. & Foster, D. J. Hippocampal place-cell sequences depict future paths to remembered goals. *Nature* **497**, 74-79 (2013).

47 Buzsaki, G. *et al.* Tools for probing local circuits: high-density silicon probes combined with optogenetics. *Neuron* **86**, 92-105, doi:10.1016/j.neuron.2015.01.028 (2015).

48 Shobe, J. L., Claar, L. D., Parhami, S., Bakhurin, K. I. & Masmanidis, S. C. Brain activity mapping at multiple scales with silicon microprobes containing 1,024 electrodes. *J Neurophysiol* **114**, 2043-2052, doi:10.1152/jn.00464.2015 (2015).

bioRxiv preprint doi: https://doi.org/10.1101/242693; this version posted January 4, 2018. The copyright holder for this preprint (which was not certified by peer review) is the author/funder. All rights reserved. No reuse allowed without permission.

49 Karumbaiah, L. *et al.* Relationship between intracortical electrode design and chronic recording function. *Biomaterials* **34**, 8061-8074, doi:10.1016/j.biomaterials.2013.07.016 (2013).

50 D. Kipke, R. V., J. Williams, J. Hetke. Silicon-Substrate Intracortical Microelectrode Arrays for Long-Term Recording of Neuronal Spike Activity in Cerebral Cortex. *IEEE TRANSACTIONS ON NEURAL SYSTEMS AND REHABILITATION ENGINEERING* **11**, 151-155 (2003).

51 Okun, M., Lak, A., Carandini, M. & Harris, K. D. Long Term Recordings with Immobile Silicon Probes in the Mouse Cortex. *PLoS One* **11**, e0151180, doi:10.1371/journal.pone.0151180 (2016).

52 Jun, J. J. *et al.* Real-time spike sorting platform for high-density extracellular probes with ground-truth validation and drift correction. *bioRxiv*, doi:https://doi.org/10.1101/101030 (2017).

53 Wassum, K. M. *et al.* Silicon Wafer-Based Platinum Microelectrode Array Biosensor for Near Real-Time Measurement of Glutamate in Vivo. *Sensors (Basel)* **8**, 5023-5036, doi:10.3390/s8085023 (2008).

54 Wu, F. *et al.* Monolithically Integrated muLEDs on Silicon Neural Probes for High-Resolution Optogenetic Studies in Behaving Animals. *Neuron* **88**, 1136-1148, doi:10.1016/j.neuron.2015.10.032 (2015).

55 Tooker, A. *et al.* Microfabricated Polymer-Based Neural Interface for Electrical Stimulation/Recording, Drug Delivery, and Chemical Sensing - Development. *Ieee Eng Med Bio*, 5159-5162 (2013).

56 Le Guehennec, L., Soueidan, A., Layrolle, P. & Amouriq, Y. Surface treatments of titanium dental implants for rapid osseointegration. *Dent Mater* **23**, 844-854, doi:10.1016/j.dental.2006.06.025 (2007).

57 Matsumura, H. & Nakabayashi, N. Adhesive 4-META/MMA-TBB opaque resin with poly(methyl methacrylate)-coated titanium dioxide. *J Dent Res* **67**, 29-32, doi:10.1177/00220345880670010501 (1988).

58 Cheng, S. & Frank, L. M. New experiences enhance coordinated neural activity in the hippocampus. *Neuron* **57**, 303-313, doi:10.1016/j.neuron.2007.11.035 (2008).

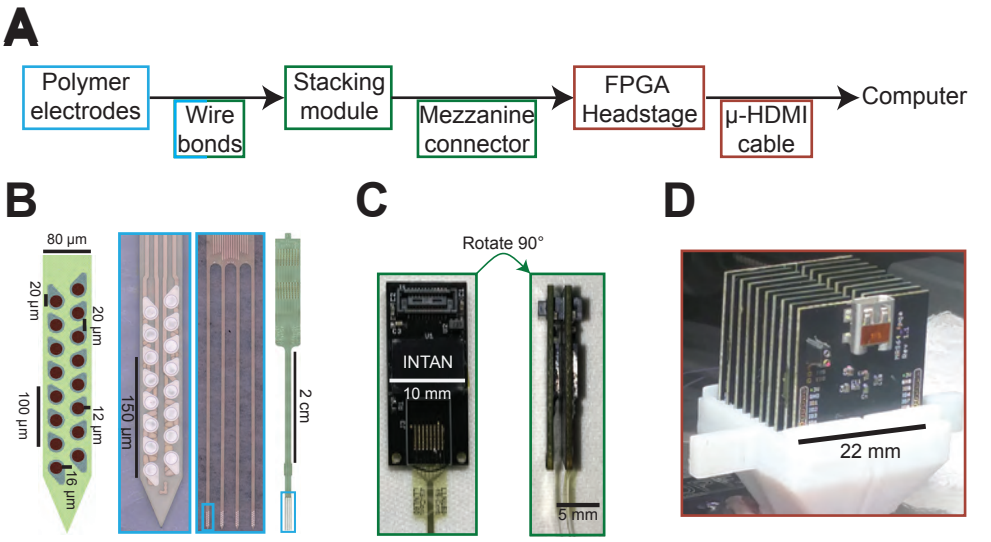
A
Polymer electrodes
Wire bonds
Stacking module
Mezzanine connector
FPGA Headstage
μ-HDMI cable
Computer
B
80 μm
20 μm
20 μm
100 μm
12 μm
16 μm
150 μm
2 cm
C
Rotate 90°
INTAN
10 mm
5 mm
D
22 mm

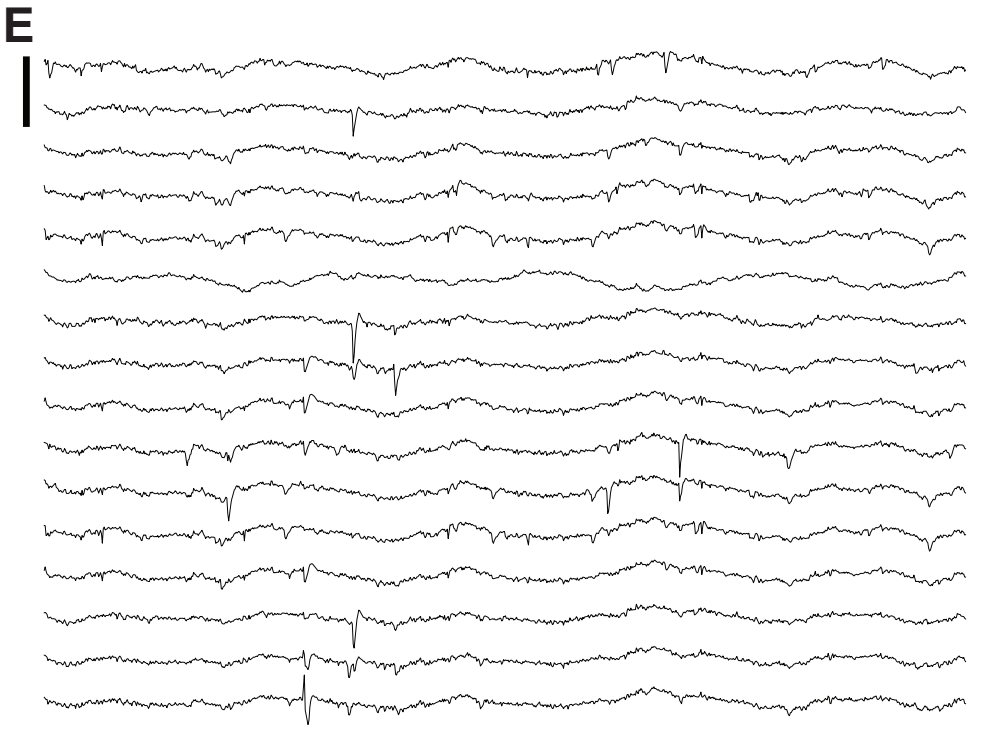
E

Figure 1

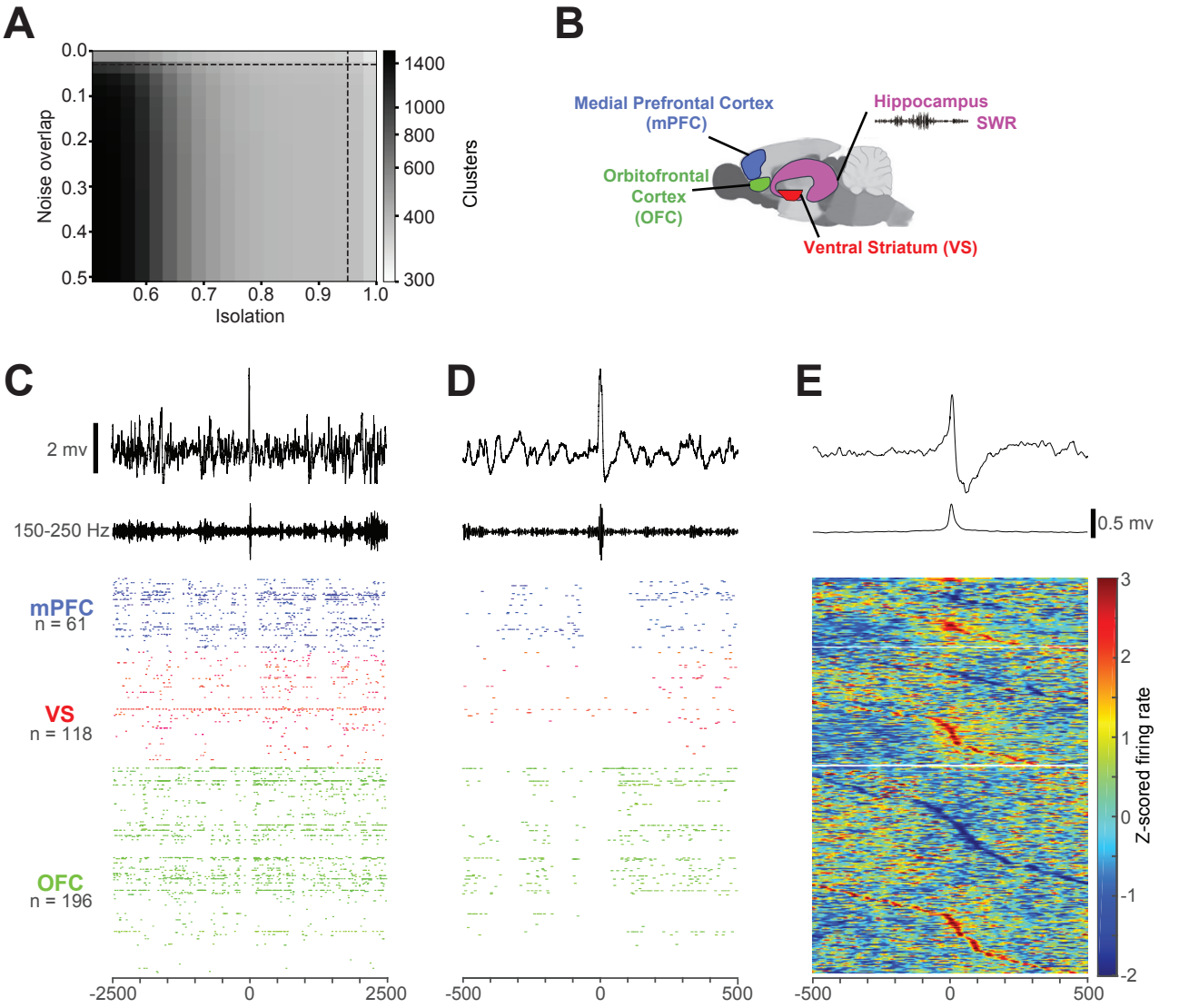
A
Noise overlap
Isolation
Clusters
B
Medial Prefrontal Cortex (mPFC)
Hippocampus
SWR
Orbitofrontal Cortex (OFC)
Ventral Striatum (VS)
C
2 mv
150-250 Hz
mPFC
n = 61
VS
n = 118
OFC
n = 196
D
E
0.5 mv
Z-scored firing rate

Figure 2

bioRxiv preprint doi: https://doi.org/10.1101/242693; this version posted January 4, 2018. The copyright holder for this preprint (which was not certified by peer review) is the author/funder. All rights reserved. No reuse allowed without permission.

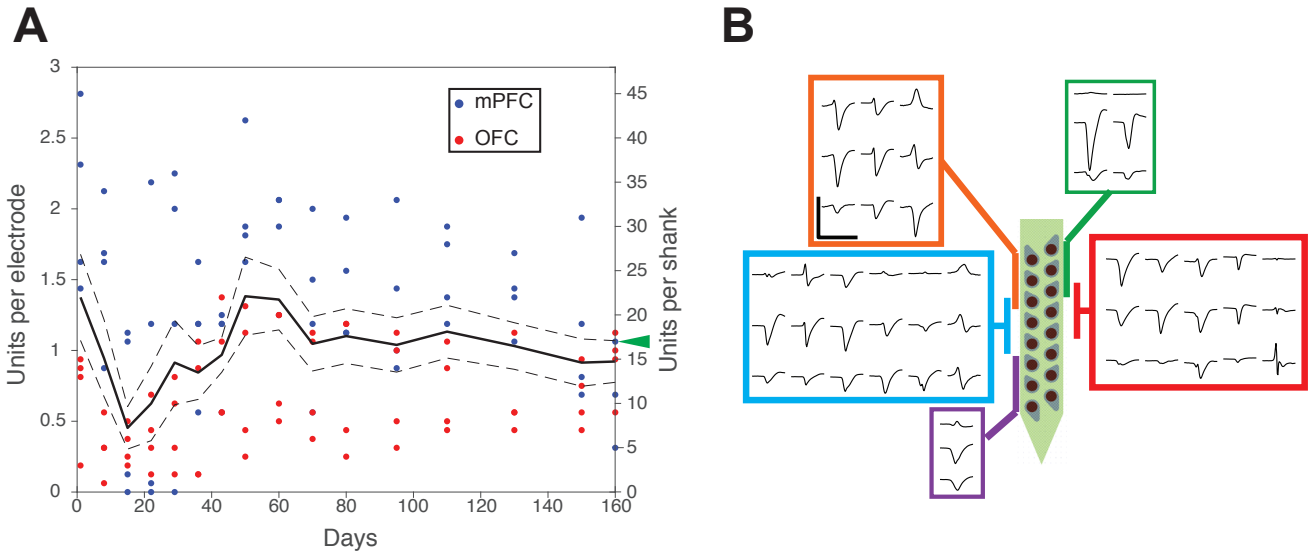

Figure 3

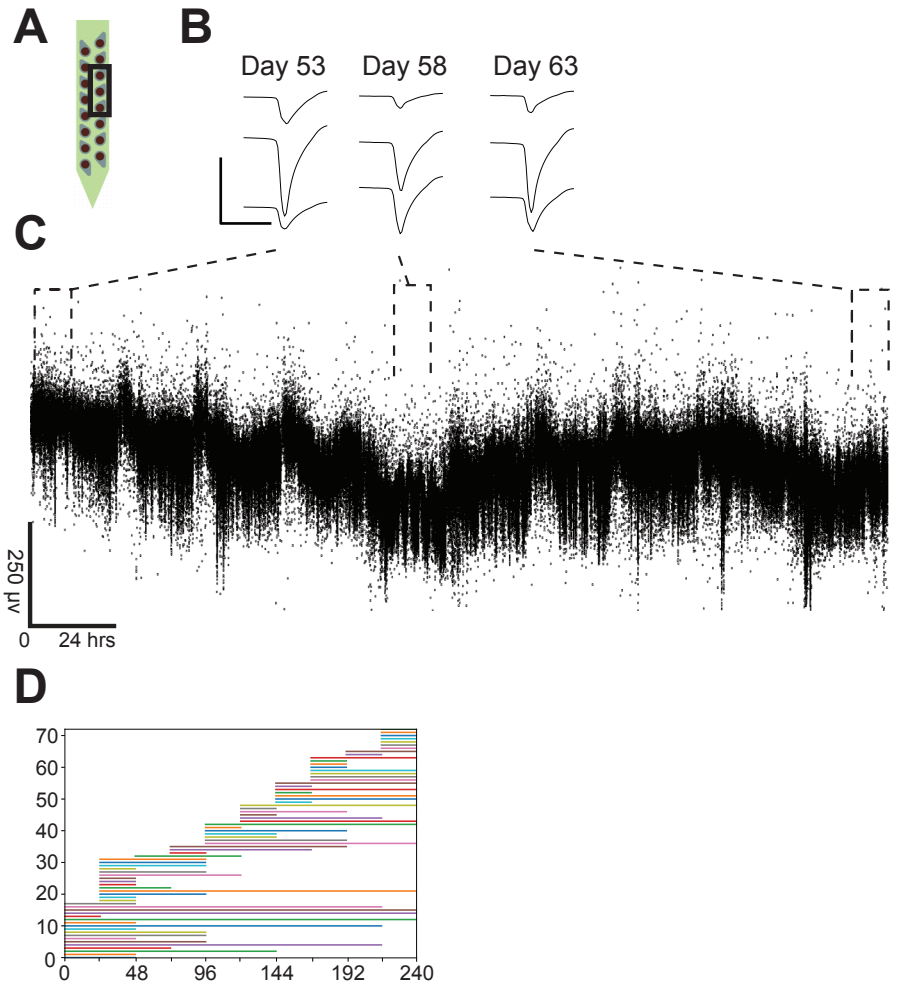
A
B
Day 53
Day 58
Day 63
C
250 µv
0
24 hrs
D
70
60
50
40
30
20
10
0
0
48
96
144
192
240

Figure 4

bioRxiv preprint doi: https://doi.org/10.1101/242693; this version posted January 4, 2018. The copyright holder for this preprint (which was not certified by peer review) is the author/funder. All rights reserved. No reuse allowed without permission.

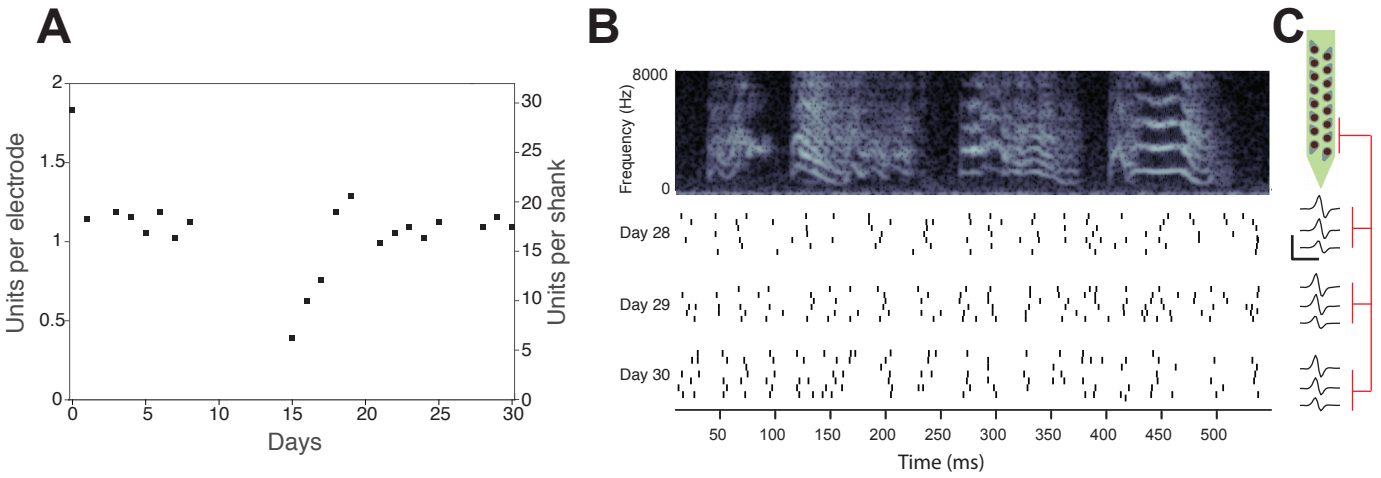

Figure 5

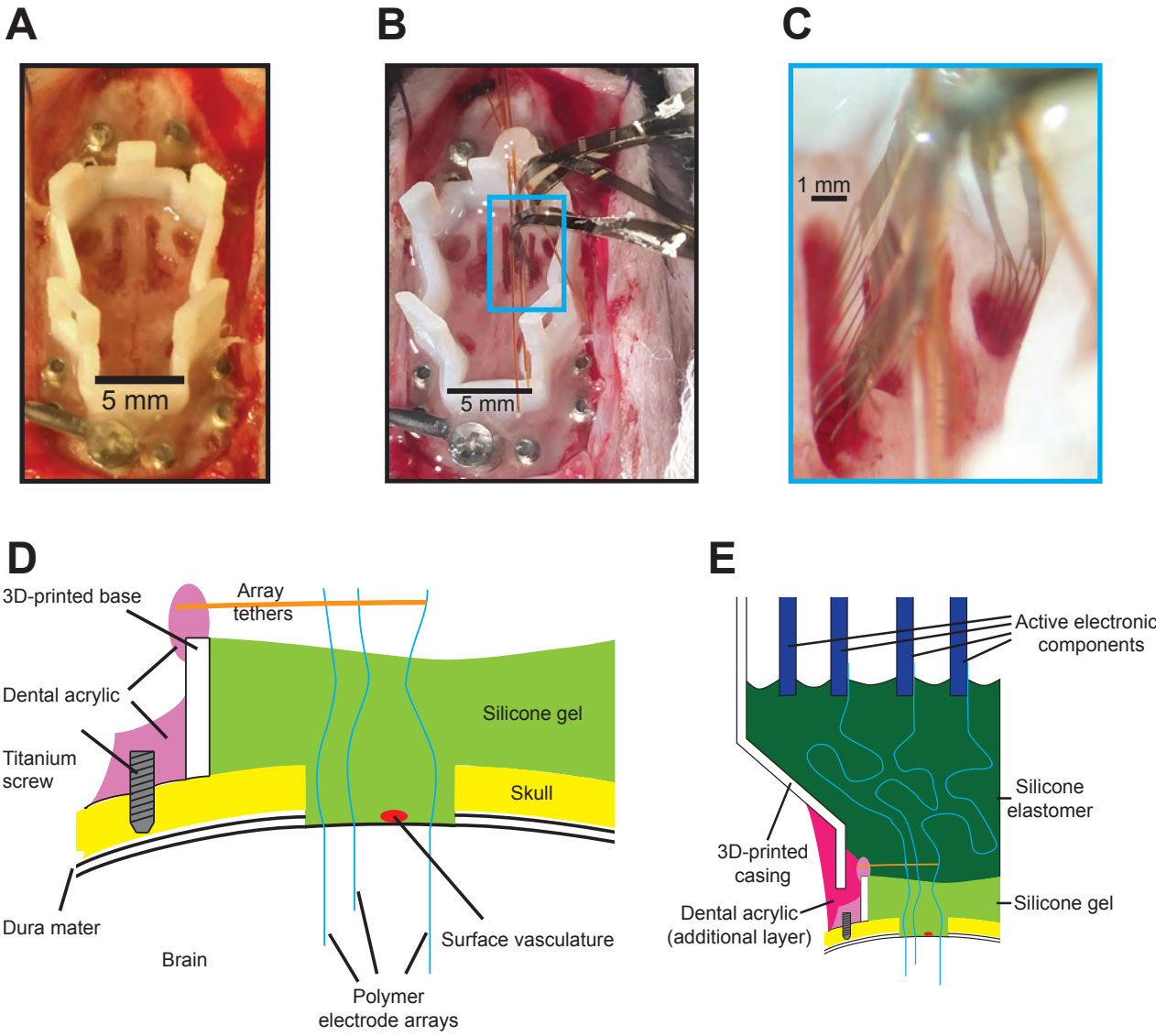

Supplemental Figure 1

bioRxiv preprint doi: https://doi.org/10.1101/242693; this version posted January 4, 2018. The copyright holder for this preprint (which was not certified by peer review) is the author/funder. All rights reserved. No reuse allowed without permission.

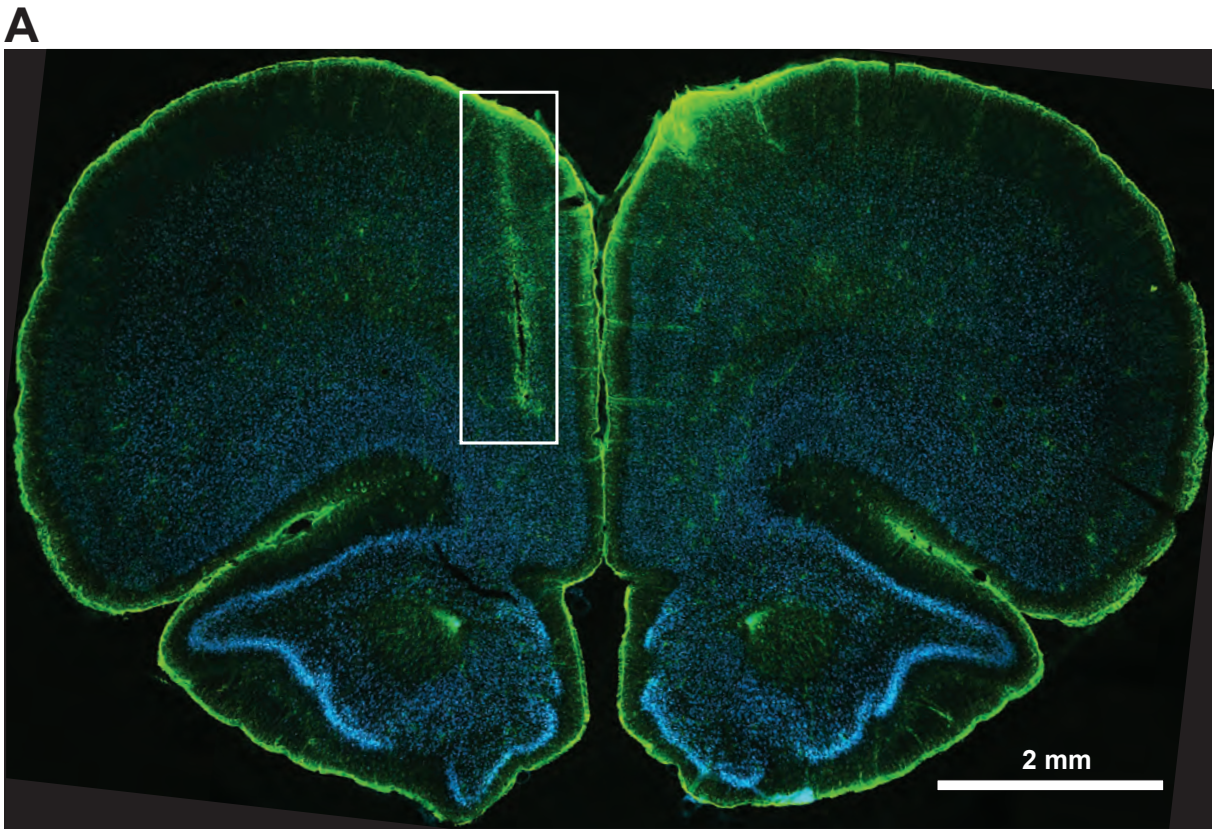

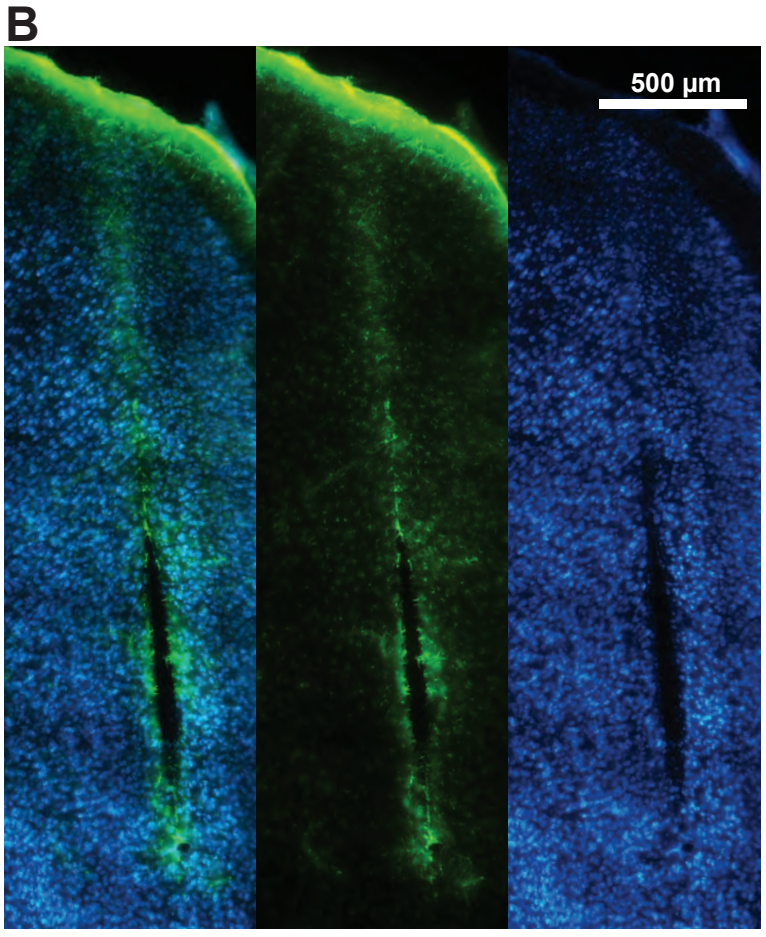

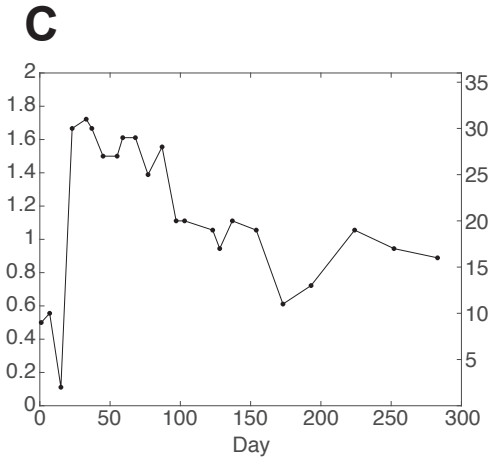

Supplementary Figure 2

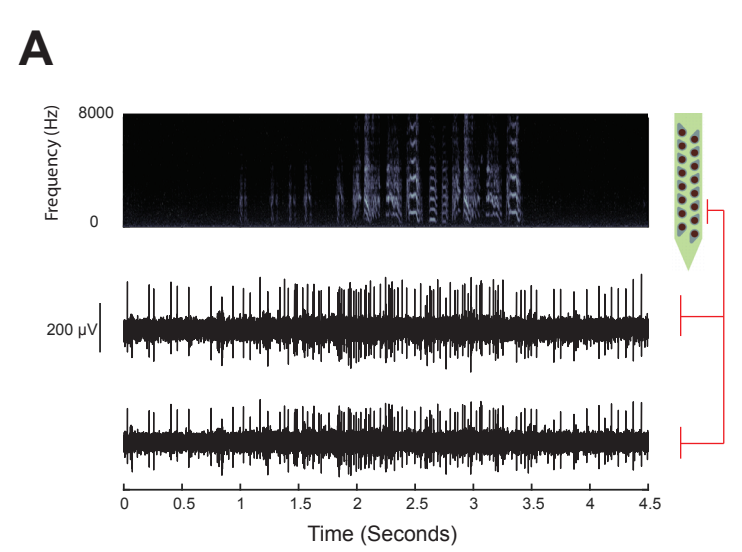

Supplemental Figure 3